Available online at www.sciencedirect.com
ScienceDirect
Trans. Nonferrous Met. Soc. China 25(2015) 3685−3693
Transactions of Nonferrous Metals Society of China
www.tnmsc.cn

Preparation of ultra-fine grain Ni−Al−WC coating with interlocking bonding on austenitic stainless steel by laser clad and friction stir processing

Yong-jun XIONG[1], Zi-li QIU[1], Rui-di LI[1,2], Tie-chui YUAN[1], Hong WU[1], Jin-hui LIU[3]

1. State Key Laboratory of Powder Metallurgy, Central South University, Changsha 410083, China;
2. State Key Laboratory of Materials Processing and Die & Mould Technology, Huazhong University of Science and Technology, Wuhan 430074, China;
3. Modern Manufacture Center, Heilongjiang University of Science and Technology, Harbin 150027, China

Received 26 June 2014; accepted 6 September 2015

Abstract: The ultra-fine structured Ni−Al−WC layer with interlocking bonding was fabricated on austenitic stainless steel by combination of laser clad and friction stir processing (FSP). Laser was initially applied to Ni−Al elemental powder preplaced on the austenitic stainless steel substrate to produce a coating for further processing. The as-received coating was subjected to FSP treatment, processed by a rotary tool rod made of WC−Co alloy, to obtain sample for inspection. Microstructure, phase constitutions, hardness and wear property were investigated by methods of scanning electronic microscopy (SEM) with energy-dispersive X-ray spectroscopy (EDX) microanalysis, and X-ray diffraction (XRD), hardness test alongside with dry sliding wear test. The results show that the severe deformation effect exerted on the specimen resulted in an ultra-fine grain layer of about 100 μm in thickness and grain size of 1−2 μm. Synergy between introduction of WC particles to the deformation layer and deformation strengthening contributes greatly to the increase in hardness and friction resistance. An interlocking bonding between the coating and matrix which significantly improves bonding strength was formed due to the severe deformation effect.

Key words: laser clad; friction stir processing; Ni−Al−WC coating; ultra-fine grain; interlocking bonding

1 Introduction

Ultra-fine grain materials exhibit significantly excellent performance over the traditional one with coarse grain. Most of the failure during the service of materials occurs on the surface of work pieces. For this reason, preparation of ultra-fine grain coating is necessary to improve the performance of substrate. Laser cladding is a surface treatment technique which employs laser beam as heat source to form metallurgical bonding between the matrix and coatings. Some researchers have covered the study of laser cladding coating on surface treatment [1−5]. There are two major concerns in the research of laser clad coating on austenitic stainless steel: one is how to refine the grain of coating from coarse size to the fine-grain and even to the nano-scale [6−11], thus a more desirable performance can be obtained; the other is what can be done to improve the bonding condition between the matrix and surface material, hence, to avoid distinct transition section or thermo-match degeneration in materials which may lead to crack formation and short life span.

To overcome the disadvantages of laser cladding, friction stir processing (FSP) becomes a superb choice amongst others. FSP is a thermomechanical treatment during which the workpiece undergoes severe plastic deformation at high temperatures. Materials can reach the ultra-fine even to the nano scale after the treatment of FSP with enhanced mechanical performance. Currently, FSP has mainly focused on the microstructural refinement of soft metals, for instance, Mg alloys [12,13] and Al alloys [9,10,14−16]. Some FSP works focused on high-strength materials such as stainless steel [17,18],

Foundation item: Projects (51571214, 51301205, 51101126) supported by the National Natural Science Foundation of China; Project (P2014-07) supported by the Open Fund of State Key Laboratory of Materials Processing and Die & Mould Technology, China; Project (20130162120001) supported by the Specialized Research Fund for the Doctoral Program of Higher Education of China; Project (K1308034-11) supported by the Changsha Municipal Science and Technology Plan, China; Projects (2015GK3004, 2015JC3006) supported by the Science and Technology Project of Hunan Province, China; Project supported by the Innovation-driven Plan in Central South University, China; Project supported by the Independent Project of State Key Laboratory of Powder Metallurgy of Central South University, China
Corresponding author: Tie-chui YUAN; Tel: +86-731-88830142; E-mail: tiechuiyuan@csu.edu.cn; Rui-di LI; E-mail: liruidi@csu.edu.cn;
DOI: 10.1016/S1003-6326(15)64009-2

tool steel [7,19], coating [7,20,21]. Therefore, FSP is an ideal way for microstructural refinement and forming interlocking bonding of coating.

In this work, we concentrate on preparation of Ni−Al coating with ultra-fine grain and interlocking bonding with substrate by laser clad and friction stir processing. In the meantime, by using a WC−Co FSP tool, we try to introduce a certain amount of WC particles into the coating, which act as a dispersoid hard phase so as to obtain better wear resistance. The microstructural evolution of as-received Ni−Al−WC coating and matrix was investigated. Mechanical properties and tribology characteristics were also characterized.

2 Experimental

The stainless steel substrate (100 mm × 60 mm × 10 mm) for laser cladding was acquired from cutting off a continuous plate. The substrate was machined on the surface and blasted with sand to remove impurities and oxide before laser cladding. The nominal chemical composition of Ni−Al alloy powder is 80% Ni and 20% Al (mass fraction). The 304 stainless steel used in the experiment consists of 0.06% C, 0.48% Si, 1.54% Mn, 18.47% Cr, 8.3% Ni, 0.37% Cu, 0.027% Nb, 0.30% Mo (mass fraction) and Fe in balance.

In laser surface cladding (LSC) experiments, the heat source is a pulsed Nd:YAG laser with maximum output power of 400 W. Computer aided multiaxis positioning system and worktable cooperate with the laser. A rectangular pulse was applied to obtaining steady square wave pulse. A focus lens with a focal distance of 100 mm focused the spot size of laser beam to approximately 1.5 mm. Uniform powder beds were applied to increasing the laser energy absorptivity of 304 stainless steel surface.

After laser cladding experiments, FSP was applied to the laser-clad Ni−Al coating. The FSP tool rod was made of WC−Co hard metal in a columnar shape with the diameter of 10 mm without a probe. The adopted rotation speed was 1000 r/min with travel speed of 50 mm/min. Optical microscopy observation proved that there were no detectable cracks on the surface after FSP.

After FSP, transverse cross sections were obtained from the specimens for microstructure and microhardness examination. The cross section of FSP samples was observed by scanning electron microscope (SEM, JEOL JSM−6700) equipped with an energy-dispersive spectroscope (EDS). The phases before and after FSP were inspected by X-ray diffraction (XRD) with Cu K_α radiation.

Surface layer microhardness test was carried out by a micro-Vickers hardness tester with an applied load of 300 g for 10 s. Wear resistances of Ni−Al based coatings before and after FSP were conducted on the UMT-2MT tribo-meter with ball-on-disk configuration without lubrication. The ball material was quenched chromium steel with a Rockwell hardness of 60−63 and a diameter of 9.5 mm. The disk was vertically fixed while the ball can reciprocally slide on the disk. The tests were conducted at room temperature with a fixed load of 5 N. The morphology of the as-received sample was characterized by SEM.

3 Results and discussion

3.1 Characterization of ultra-fine grain surface layer

Figure 1 shows the XRD patterns of laser clad Ni−Al−WC coating before and after the FSP. The strong diffraction peaks presenting the $Al_{0.9}Ni_{1.1}$ can be observed evidently in both curves. Moreover, there are diffraction peaks of $AlNi_3$. However, there are two new phases, tungsten carbide (WC) and Fe−Ni, appearing after friction stir processing. It was reasonable to conclude that WC was incorporated in Ni−Al coating during friction stir processing since the FSP tool was made by WC−Co. Both the rotary tool rod and the Ni−Al coating were subjected to high temperature and intense stress during the FSP treatment. As the tool rod, made of WC cemented with Co, would inevitably wear off in this process, the abrasive dust consisting of WC and Co subsequently entered the coating layer. Under the influence of high temperature and severe deformation, the particles of WC entered the surface of the coating and blended into coating layer. These dispersed WC particles resulted in a dispersion strengthening effect, which helps to improve the strength and hardness of the coating, thus prolongs the service life of the whole workpiece. As for the Fe−Ni diffraction pattern, the severe friction exerted by the rotary rod affected not only the coating itself, but

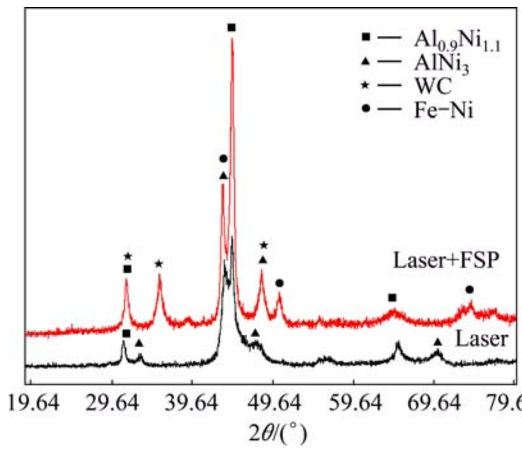

Fig. 1 XRD patterns obtained from unattended laser cladding and FSP-treated coating

also the inner austenitic steel matrix, and the Fe and Ni atoms were brought from the substrate to the surface coating. More specifically, $Al_{0.9}Ni_{1.1}$ diffraction peak shifted to the higher angle after FSP, as shown in Fig. 2. According to the well-known Bragg equation, this indicates that the lattice parameter was decreased after FSP. Meanwhile, there is a slight augmentation in the full-width at half-maximum (FWHM) of the peaks, which is accounted for the evidence of grain refinement. This is because the rotation friction can be treated as severe plastic deformation (SPD) which can refine microstructure and form plastic zone. In the rotary friction process, the extremely high strain rate would not provide sufficient time for the growth of nuclei formed from dynamic recrystallization (DRX), yielding the ultra-fine grains. Additionally, when the dramatic plastic deformation (hardening) occurs with insufficient softening, the crystal lattice will be disintegrated into disorderliness [20].

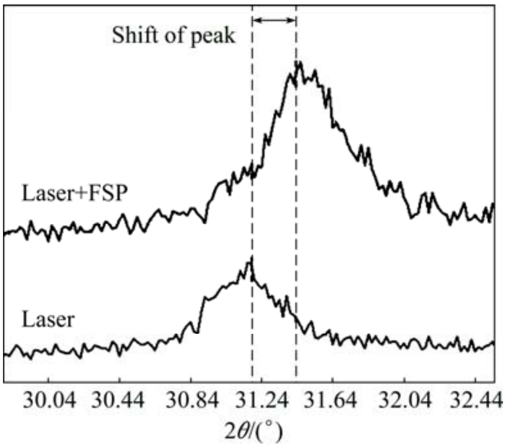

Fig. 2 Magnified XRD pattern of unattended laser cladding and FSP-treated coating from 30° to 32° showing shift of peak after processing

Figure 3 shows the typical microstructure of laser cladding Ni−Al alloy coating from the cross section view. The microstructure showed dendritic and cellular crystals with grain sizes of 2−3 μm. The laser cladding alloy coating also showed well metallurgical connection between steel substrate with smooth epitaxial solidification interface. Figure 4 shows the typical microstructure of laser-clad Ni−Al coating after friction stir processing from cross section view. Obviously, there are three zones: 1) the top surface of SPD zone, more closely shown in Fig. 4(b), which had underwent the most severe plastic deformation and following dynamic recrystallization (DRX), in which equiaxed ultra-fine grains were developed. The grain size in this section is 1−2 μm; 2) the thermo-mechanically affected zone underneath the SPD zone, where the material was subjected to plastic deformation and friction heat. Due

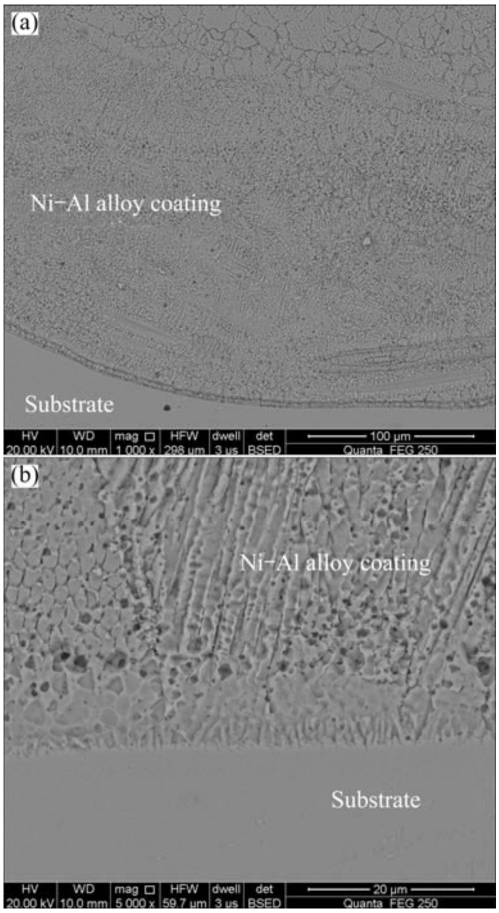

Fig. 3 SEM images of typical microstructure of Ni−Al coating by laser cladding

to the insufficient force and strain, the coarse grains were just compressed and extruded into lath-shaped, then hardened, as depicted in Fig. 4(c); 3) Figure 4(d) shows the original laser clad zone with relatively coarse grains, where the grains are nearly in their primitive state, but, we can still find that the texture is observable. Compared to the other two zones, this section is exposed to the minimum external force and heat flux. Thus, the basic morphology did not change obviously. However, through the texture of the image, it is not difficult to find that there indeed is some extent of deformation. Interestingly, the interlocking boundary between the coating and austenitic steel matrix can be found, which is due to the plastic flow and interpenetrations at the interface of coating and matrix.

Figure 5 presents the transition area between SPD zone and thermal-mechanically affected zone. The top surface zone is featured by the severely deformed then recrystallized ultra-fine grain with streamline parallel to the upper plane. In addition, the gradient grain from top surface to the inner layer can be found, showing the microstructure gradual evolution from top to bottom, which guarantees better mechanical resistance when subjected to impact.

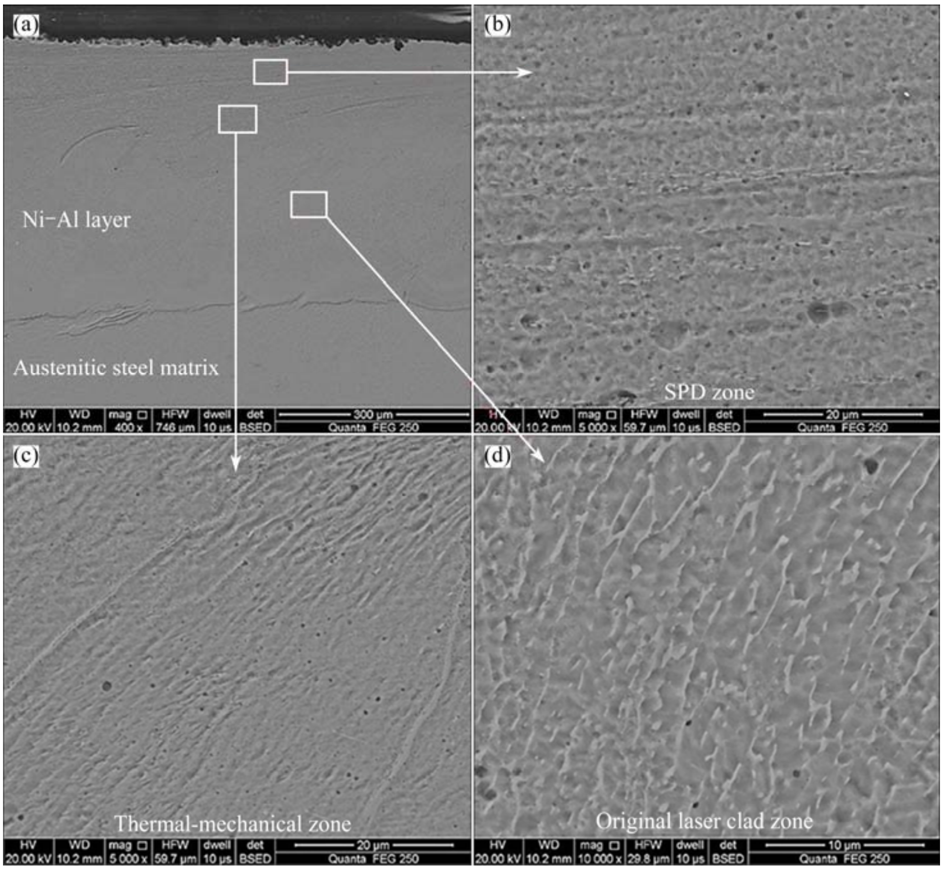

Fig. 4 SEM images of characteristic microstructures of rotation friction processed laser coating: (a) Low magnification, showing both Ni−Al coating layer and austenitic steel matrix; (b) Severe plastic deformation (SPD) zone close to surface of coating; (c) Thermal-mechanical zone approximately 200 μm under SPD zone; (d) Original laser-clad zone with coarse grain

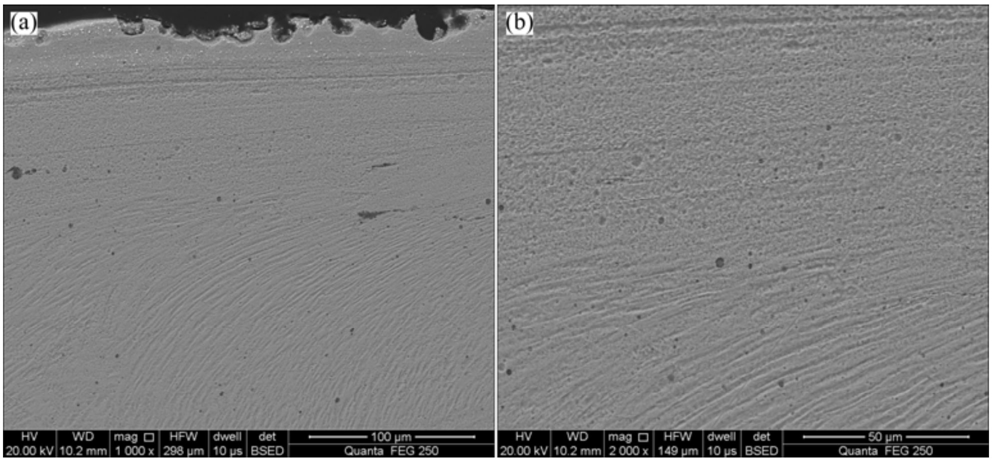

Fig. 5 SEM images of transition area between SPD zone and thermal-mechanical zone

Grain size variation from top surface to the inside of Ni−Al−WC coating is presented in Fig. 6. Within 100 μm from surface, the grain size is almost less than 2 μm, majorly 1 μm. This demonstrates that the thickness of SPD zone is around 100 μm. From 100 to 180 μm, in which thermal-mechanical zone lies, the grain size grows exponentially fast, from 2 to 7 μm. Under 200 μm, the curve of grain size-depth becomes flat and reaches the plateau. In original laser clad zone, grain size stays at about 8 μm.

Figure 7 illustrates the interlocking structure of as-received Ni−Al−WC coating and substrate. It can be found that in Fig. 7(b), the boundary between the coating layer and austenitic steel matrix does not stay flat as that before FSP, but in a folded configuration which we call interlocking bonding structure. The top surface of the Ni−Al−WC coating experienced the most severe plastic deformation in FSP. For the reason that Co-based alloy

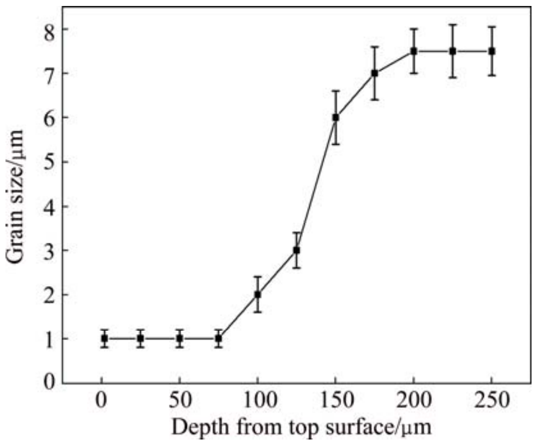

Fig. 6 Grain size variation from top surface to inside of coating

has a low stacking fault energy (SFE) [22], the dynamic recrystallization (DRX) serves as the main deformation mechanism. Hence, the grains of coating on top surface were crushed into finer ones, which is why DRX could dramatically refine the microstructure. However, visible variation of grain size only observed on top surface does not necessarily suggest that there was only deformation within 100 μm thickness on top. Similar deformation could also take place both in thermal-mechanical zone and original laser-clad zone, in a less severe manner. Though not intense enough to cause remarkable refinement on the size of grains, the texture shown in lower half of picture of Fig. 5 could verify the existence of such deformation. At the conjunction of coating and austenitic steel matrix substrate, two types of materials were forced to overlap and thus interlocking bonding structure formed during the deformation process. Apparently, such structure is favorable for the bonding strength of the coating−matrix interface. With the combination of both mechanical and metallurgical bondings, the interlocking structure is beneficial for the coating to prevent the crack initiation at interface and serve in the hardest environment. Moreover, Fig. 7(c) shows the formation of ultrafine grain in the austenitic steel matrix at the interlocking bonding section. Figure 7(d) presents the original coarse grain of steel matrix. During FSP, the effect of severe plastic deformation strongly refines the grain and forms high density dislocation, non-equilibrium grain- boundary. Hence, not only the laser clad Ni−Al−WC coating, but also the matrix austenitic steel was plastically deformed with enhanced performance.

Energy-dispersive X-ray spectroscopy microanalysis (EDX) was conducted to determine the elements

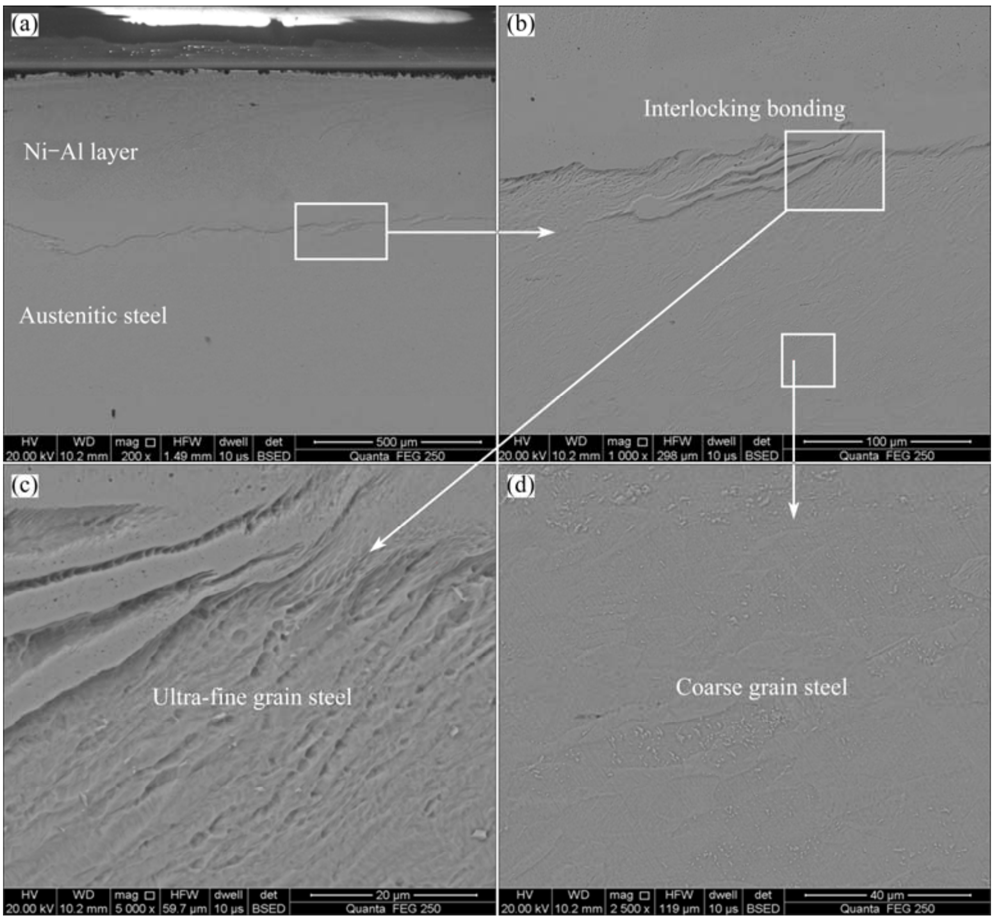

Fig. 7 SEM images for boundary between coating layer and austenitic steel matrix (a), interlocking bonding section (b), austenitic steel forming ultrafine grain (c) and original coarse grain steel (d)

distribution across the interlocking boundary with the result shown in Fig. 8. Within 20 μm range around the interlocking boundary, the main elements are Al, Cr, Fe and Ni. At Ni−Al−WC coating side, all four elements can be detected. The Ni composes over 35% in this section which is equal to the content of Fe. Al has about 21% and Cr has the lowest content of 8%. At the side of austenitic steel matrix, the contents of Ni and Al fall to zero. Cr content rises to above 15% while Fe has the highest content of over 80%. The sufficient diffusion of atoms across the boundary section guarantees desirable bonding between the coating and steel matrix.

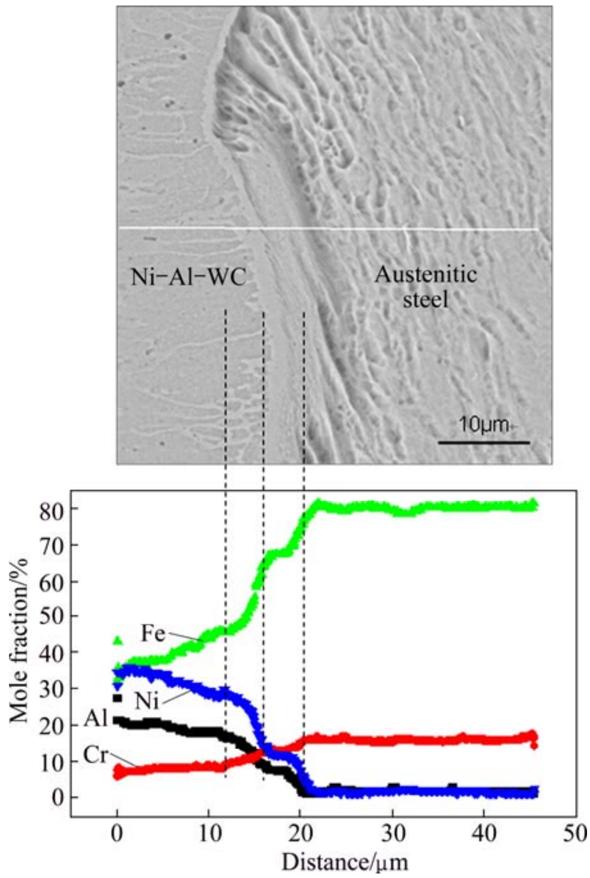

Fig. 8 EDS line scanning plot for elements distribution near interlocking binding boundary

3.2 Microhardness and tribology behavior

Figure 9 shows the variation of microhardness with the distance from the top surface of Ni−Al−WC coating to austenitic steel matrix after FSP. The change of hardness from top surface to the matrix indicated that the thickness of ultrafine layer combining thermal-mechanical zone was 150−200 μm. The maximal microhardness was HV 715 while the microhardness in the range of 300−700 μm is about HV 500. The apparent increase of microhardness found in surface is due to the severe plastic deformation during FSP. Coarse grains were shattered under the influence of high gradient temperature, stress−strain, and accordingly complex grain crushing and dynamic recrystallization. According to the Hall−Petch equation, changing grain size in a certain range can influence dislocation movement and yield strength. Thus, a more favorable mechanical performance is obtained by crushing coarse grains into finer ones. Another factor contributing to the elevating microhardness is the additional WC particles from the FSP rotary tool rod during the process. WC shows extremely high hardness and elastic modulus, acting as an excellent second phase particle which enhances the strength of the coating by pinning the grain boundary and inhabiting the growth of grains. In Fig. 7, SEM images show that the thickness of the entire laser clad Ni−Al−WC coating is about 500 μm. Therefore, both the strain hardening and the incorporation of WC particle lead to the highest hardness on top surface. At the depth of 700 μm, the matrix steel shows the hardness of HV 500. From 700 to 1000 μm, the hardness decreases gradually.

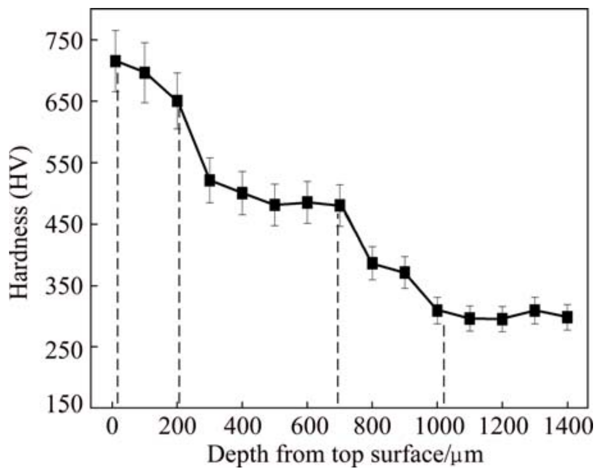

Fig. 9 Microhardness depth profile of cross section of as-received laser-clad Ni−Al−WC coating

3.3 Friction behavior

3.3.1 Friction coefficient

The friction coefficients between laser clad coating and cemented carbide under different rotary speeds are depicted in Fig. 10. The plot exhibits the friction coefficient of laser clad coating before and after FSP procedure. There are two stages for both curves: from 0 to 200 s, the friction coefficient increases gradually; after exceeding 200 s, curves come to a plateau and keep steady relatively with only small range of oscillation. The starting point of unattended sample is lower than that of the as-received coating; each begins from 0.127 to 0.177 while after 200 s, the curve of FSP-treated sample has raised over the laser-clad-only sample. It can also be found that the friction coefficient is increased after FSP because of the introduction of WC during the FSP process. After FSP, the surface layer is transformed into

Ni−Al−WC composites, which is different from the original Ni−Al alloy layer. Although the friction coefficient is increased, the wear resistance of FSP-treated layer is enhanced due to the dispersed hard WC particles. Therefore, it is not contradict that the wear performance is enhanced after FSP.

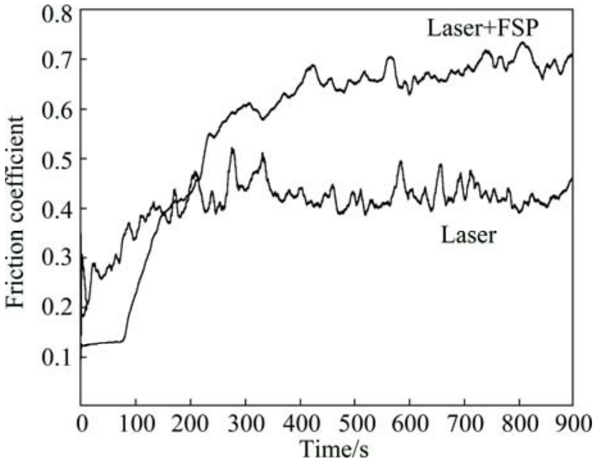

Fig. 10 Friction coefficient—time curves between cemented carbide and laser-clad coating

Figure 11 shows the wear depth comparison of two coating samples with different treatments after the friction test. The depth of wear loss of sample with laser clad reached over 32 μm while that of the FSP one was only 15 μm. With great increase in hardness by ultra-fine grain strengthening and WC particulate reinforcement, we can conclude that FSP-treated laser clad Ni−Al−WC coating possesses much more desirable wear resistance compared to the one without FSP.

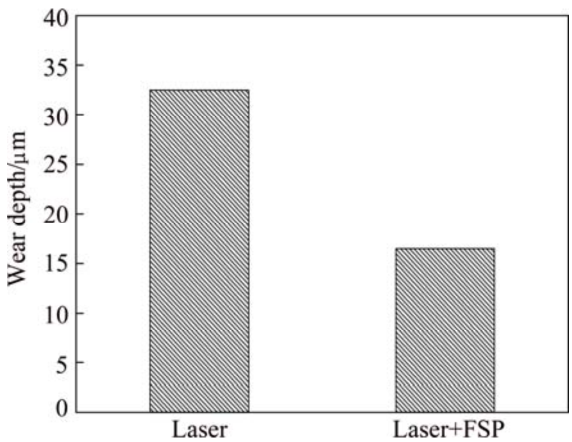

Fig. 11 Wear depth comparison after friction test

3.3.2 Morphology of laser clad coating surface after FSP

Figure 12(a) shows the apparent parallel grooves on worn surface representing the abrasion wear. The presence of exfoliation in the view of grooves indicated the local friction deformation and plowing during sliding. For the worn surface of FSP-treated sample shown in Fig. 12(b), it became very smooth and hardly no exfoliation can be found. It is reasonable to believe that the friction mechanism shifts from abrasion wear of laser-clad-only sample to the adhesion wear in FSP. This transformation is favorable for the increase of wear resistance.

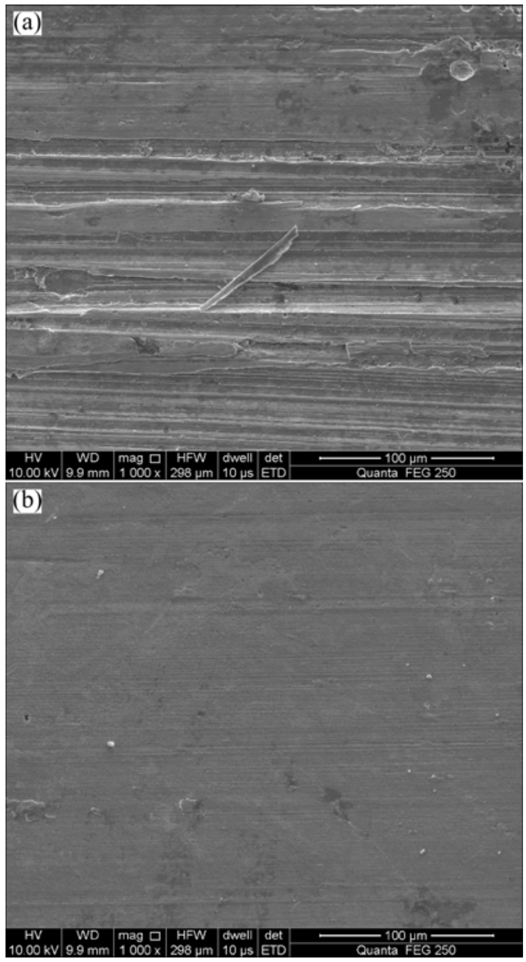

Fig. 12 SEM images showing morphology of worn surfaces: (a) Laser-clad only; (b) Laser+FSP

4 Conclusions

1) XRD analysis suggests that the phases of $Al_{0.9}Ni_{1.1}$, $AlNi_3$, WC and Fe−Ni were formed in original Ni−Al based coating after FSP procedure. A 100 μm thick ultra-fine grain layer was obtained. The microstructures of laser clad Ni−Al−WC coating were mainly composed of SPD zone, where ultra-fine grain mainly concentrated, thermal-mechanical affected zone, where grains are less refined but also with relative high hardness, and original laser clad zone.

2) The grains refinement and the introduction of WC during the FSP are prior reasons for the improvement in mechanical performance of the laser clad coating. Reduction of grain size has positive influence on the dislocation movement and yield strength.

WC particles in coating layer can impede further dislocation propagation and boundary migration. Hence, the strength and hardness of coating both increased. Synergy between two aspects resulted in an increase in hardness up to HV 715.

3) Severe plastic deformation also has impact on the austenitic steel matrix. A very strong interlocking bonding was formed at the boundary between coating and matrix. The bonding strength of coating was thus considerably increased.

4) Higher hardness improves friction resistance of as-received laser clad coating with FSP. Friction wear test result shows that it has much more favorable wear resistance than the unattended laser clad coating. Wear depth was reduced by half, from 32.5 to 16.5 μm, after FSP treatment. The mechanism of friction shifts from abrasion wear of laser-clad-only sample to adhesion wear for the FSP-treated one.

References

[1] CHONG P H, LIU Z, SKELDON P, THOMPSON G E. Large area laser surface treatment of aluminium alloys for pitting corrosion protection [J]. Applied Surface Science, 2003, 208: 399−404.

[2] TOMIDA S, NAKATA K. Fe−Al composite layers on aluminum alloy formed by laser surface alloying with iron powder [J]. Surface and Coatings Technology, 2003, 174: 559−563.

[3] YILBAS B S, ARIF A F M, KARATAS C, RAZA K. Laser treatment of aluminum surface: Analysis of thermal stress field in the irradiated region [J]. Journal of Materials Processing Technology, 2009, 209(1): 77−88.

[4] YUE T M, DONG C F, YAN L J, MAN H C. The effect of laser surface treatment on stress corrosion cracking behaviour of 7075 aluminium alloy [J]. Materials Letters, 2004, 58(5): 630−635.

[5] FENG Shu-rong, TANG Hai-bo, ZHANG Shu-quan, WANG Hua-ming. Microstructure and wear resistance of laser clad TiB−TiC/TiNi−Ti_2Ni intermetallic coating on titanium alloy [J]. Transactions of Nonferrous Metals Society of China, 2012, 22(7): 1667−1673.

[6] MEHRANFAR M, DEHGHANI K. Producing nanostructured super-austenitic steels by friction stir processing [J]. Materials Science and Engineering A, 2011, 528(9): 3404−3408.

[7] MORISADA Y, FUJII H, MIZUNO T, ABE G, NAGAOKA T, FUKUSUMI M. Fabrication of nanostructured tool steel layer by combination of laser cladding and friction stir processing [J]. Surface and Coatings Technology, 2011, 205(11): 3397−3403.

[8] MORISADA Y, FUJII H, MIZUNO T, ABE G, NAGAOKA T, FUKUSUMI M. Nanostructured tool steel fabricated by combination of laser melting and friction stir processing [J]. Materials Science and Engineering A, 2009, 505(1−2): 157−162.

[9] ZHANG Q, XIAO B L, WANG Q Z, MA Z Y. In situ Al_3Ti and Al_2O_3 nanoparticles reinforced Al composites produced by friction stir processing in an Al−TiO_2 system [J]. Materials Letters, 2011, 65(13): 2070−2072.

[10] YOU G L, HO N J, KAO P W. In-situ formation of Al_2O_3 nanoparticles during friction stir processing of Al−SiO_2 composite [J]. Materials Characterization, 2013, 80: 1−8.

[11] SALEHI M, SAADATMAND M, MOHANDESI J A. Optimization of process parameters for producing AA6061/SiC nanocomposites by friction stir processing [J]. Transactions of Nonferrous Metals Society of China, 2012, 22(5): 1055−1063.

[12] CHEN Ti-jun, ZHU Zhan-min, LI Yuan-dong, MA Ying, HAO Yuan. Friction stir processing of thixoformed AZ91D magnesium alloy and fabrication of Al-rich surface [J]. Transactions of Nonferrous Metals Society of China, 2010, 20(1): 34−42.

[13] DU Xing-hao, WU Bao-lin. Using friction stir processing to produce ultrafine-grained microstructure in AZ61 magnesium alloy [J]. Transactions of Nonferrous Metals Society of China, 2008, 18(3): 562−565.

[14] UZUN H. Friction stir welding of SiC particulate reinforced AA2124 aluminium alloy matrix composite [J]. Materials and Design, 2007, 28(5): 1440−1446.

[15] NASCIMENTO F, SANTOS T, VILACA P, MIRANDA R M, QUINTINO L. Microstructural modification and ductility enhancement of surfaces modified by FSP in aluminium alloys [J]. Materials Science and Engineering A, 2009, 506(1−2): 16−22.

[16] KURT A, UYGUR I, CETE E. Surface modification of aluminium by friction stir processing [J]. Journal of Materials Processing Technology, 2011, 211(3): 313−317.

[17] SAEID T, ABDOLLAH-ZADEH A, ASSADI H, GHAINI F M. Effect of friction stir welding speed on the microstructure and mechanical properties of a duplex stainless steel [J]. Materials Science and Engineering A, 2008, 496(1−2): 262−268.

[18] CHEN Y C, FUJII H, TSUMURA T, KITAGAWA Y, NAKATA K, IKEUCHI K, MATSUBAYASHI K, MICHISHITA Y, FUJIYA Y, KATOH J. Banded structure and its distribution in friction stir processing of 316l austenitic stainless steel [J]. Journal of Nuclear Materials, 2012, 420(1−3): 497−500.

[19] CHEN Y C, NAKATA K. Evaluation of microstructure and mechanical properties in friction stir processed skd61 tool steel [J]. Materials Characterization, 2009, 60(12): 1471−1475.

[20] LI Rui-di, LI Jing-long, LIANG Yi, JI Cheng-zhong, YUAN Tie-chui. Viscoplastic friction and microstructural evolution behavior of laser-clad Co−Cr−Ni−Mo coating [J]. Transactions of Nonferrous Metals Society of China, 2013, 23(3): 681−691.

[21] YAN H, WANG A, XU K, WANG W, HUANG Z. Microstructure and interfacial evaluation of co-based alloy coating on copper by pulsed Nd:YAG multilayer laser cladding [J]. Journal of Alloys and Compounds, 2010, 505(2): 645−653.

[22] CHIBA A, LEE S, MATSUMOTO H, NAKAMURA M. Construction of processing map for biomedical Co−28Cr−6Mo−0.16N alloy by studying its hot deformation behavior using compression tests [J]. Materials Science and Engineering A, 2009, 513−514(15): 286−293.

激光熔覆结合搅拌摩擦加工在奥氏体不锈钢表面制备超细晶互锁结构 Ni−Al−WC 涂层

熊拥军[1]，邱子力[1]，李瑞迪[1,2]，袁铁锤[1]，吴 宏[1]，刘锦辉[3]

1. 中南大学 粉末冶金国家重点实验室，长沙 410083；
2. 华中科技大学 材料成形与模具技术国家重点实验室，武汉 430074；
3. 黑龙江科技大学 现代制造工程中心，哈尔滨 150027

摘 要：在奥氏体钢表面制备具有超细晶结构且能与基体互锁的 Ni−Al−WC 涂层。首先采用激光在奥氏体钢表面熔覆 Ni−Al 涂层，然后采用搅拌摩擦加工(FSP)方法，以 WC−Co 合金为搅拌头，对激光涂层进行大变形改性，形成 Ni−Al−WC 超细晶复合涂层。采用扫描电子显微镜、X 光能量散射谱仪、X 射线多晶衍射、硬度仪及摩擦磨损试验机对样品的显微组织、相组成、硬度及摩擦磨损性能进行表征。结果表明，FSP 的大变形效应可形成晶粒尺寸为 1~2 μm、厚度为 100 μm 的超细晶层。同时，FSP 过程还可往变形层中引入 WC 颗粒，因此变形以及 WC 颗粒双重强化极大地提高了硬度和耐磨性。另外，FSP 大变形使涂层和基体之间形成互锁结构，有利于二者的结合。

关键词：激光熔覆；搅拌摩擦加工；Ni−Al−WC 涂层；超细晶；互锁结构

(Edited by Yun-bin HE)